analytical chemistry

Article

pubs.acs.org/ac

Enhanced Biosensing Resolution with Foundry Fabricated Individually Addressable Dual-Gated ISFETs

Carlos Duarte-Guevara,[†,⊥,▲] Fei-Lung Lai,[∥,▲] Chun-Wen Cheng,[∥] Bobby Reddy, Jr.,[†,⊥] Eric Salm,[‡,⊥] Vikhram Swaminathan,[§,⊥] Ying-Kit Tsui,[∥] Hsiao Chin Tuan,[∥] Alex Kalnitsky,[∥] Yi-Shao Liu,*[,∥] and Rashid Bashir*[,‡,⊥]

[†]Department of Electrical and Computer Engineering, University of Illinois at Urbana−Champaign, William L. Everitt Laboratory, 1406 West Green Street, Urbana, Illinois 61801, United States

[‡]Department of Bioengineering, University of Illinois at Urbana−Champaign, 1270 Digital Computer Laboratory, 1304 West Springfield Avenue, Urbana, Illinois 61801, United States

[§]Department of Mechanical Science and Engineering, University of Illinois at Urbana−Champaign, 1206 West Green Street, Urbana, 61801 Illinois, United States

[∥]Taiwan Semiconductor Manufacturing Company, 9 Creation Rd, Hsinchu Science Park, Hsinchu, Taiwan 300-77, R.O.C.

[⊥]Micro and Nanotechnology Lab, University of Illinois at Urbana−Champaign, 208 North Wright Street, Urbana, Illinois 61801, United States

S *Supporting Information*

ABSTRACT: The adaptation of semiconductor technologies for biological applications may lead to a new era of inexpensive, sensitive, and portable diagnostics. At the core of these developing technologies is the ion-sensitive field-effect transistor (ISFET), a biochemical to electrical transducer with seamless integration to electronic systems. We present a novel structure for a true dual-gated ISFET that is fabricated with a silicon-on-insulator (SOI) complementary metal-oxide-semiconductor process by Taiwan Semiconductor Manufacturing Company (TSMC). In contrast to conventional SOI ISFETs, each transistor has an individually addressable back-gate and a gate oxide that is directly exposed to the solution. The elimination of the commonly used floating gate architecture reduces the chance of electrostatic discharge and increases the potential achievable transistor density. We show that when operated in a "dual-gate" mode, the transistor response can exhibit sensitivities to pH changes beyond the Nernst limit. This enhancement in sensitivity was shown to increase the sensor's signal-to-noise ratio, allowing the device to resolve smaller pH changes. An improved resolution can be used to enhance small signals and increase the sensor accuracy when monitoring small pH dynamics in biological reactions. As a proof of concept, we demonstrate that the amplified sensitivity and improved resolution result in a shorter detection time and a larger output signal of a loop-mediated isothermal DNA amplification reaction (LAMP) targeting a pathogenic bacteria gene, showing benefits of the new structure for biosensing applications.

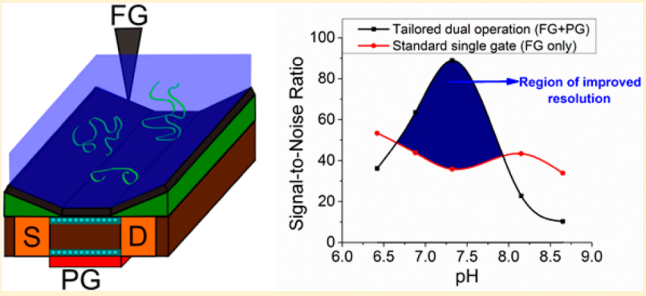

Invented in the 1970s, ISFETs have become effective transducers that convert biochemical reactions into electrical signals.[1,2] In an ISFET, the gate region is exposed to an electrolyte, making the drain-source current sensitive to charged molecules and chemical reactions in the solution.[3] These devices promise to enable multiplexed, label-free, inexpensive, and portable diagnostic tools by translating advances of the semiconductor industry to health-care and biological applications.[4] Different studies have applied the concept of electrical biosensing through field-effect and capacitive coupling for multiple purposes. Silicon nanowire transistors have been used for the detection of specific analytes in low concentrations,[5−7] carbon nanotubes and graphene FETs are being used as gas and molecular sensors,[8,9] and ISFETs made with metal oxides and polymers are used to monitor biological activity.[10−12] The potential advantage of having label-free, multiplexed, and miniaturized biosensors incentivizes research in ISFETs and its multiple variations.[13,14]

Detection of analytes at very low concentrations and analysis of biochemical reactions that provide small signals have driven research toward signal enhancement techniques for ISFET sensing. Researchers have attached particles or enzymes to analytes,[15,16] applied surface treatments to the sensor's passivation layer to control wettability,[17] and used complementary electrokinetic structures to increase local concentration,[18] all to enhance the biological signals and enable more

Received: May 21, 2014
Accepted: July 23, 2014
Published: July 23, 2014

   dx.doi.org/10.1021/ac501912x | *Anal. Chem.* 2014, 86, 8359−8367

sensitive electrical measurements. For reactions where the measured variable is the solution's pH, a number of publications demonstrated the use of coupled transistors for signal enhancement. Couples of sensors connected in parallel yield a "super-Nernstian" sensitivity that exceeds the 59 mV/pH maximum relation defined by the Nernst equation.[19] This method is particularly relevant for semiconductor DNA sequencing,[20] label-free gene detection,[21] or electrochemical-based diagnostics,[22] where accurate measurement of small pH changes is critical to minimize error rates, reduce detection limits, and improve throughput. Our group has reported coupling of nanowire and nanoplate transistors with different W/L ratios to amplify pH signals,[23] but the most common and notable coupling mechanism is the dual-gated field-effect transistor (DGFET).[24−26] Transistors fabricated from silicon-on-insulator (SOI) wafers have a top gate that is formed by depositing a dielectric on the active silicon layer and a bottom gate where the dielectric is the SOI buried oxide. When the active silicon is considerably thicker than the maximum depletion layer, there is no charge coupling between gates, and the bottom and top transistors can be treated as independent parallel devices.[27] When the top and bottom transistors are coupled in a dual-gate mode operation, their geometrical and electrical properties will produce an amplification of the pH sensitivity.[28]

In this article, we present a new structure for double-gated ISFETs that have individually addressable back-gates, overcoming limitations from the single back node of other SOI processes. In a regular SOI process, all transistors have a common back-gate that is biased through the bulk silicon. Having a common back-gate prevents tailored biasing of individual transistors that is important to operate in optimum conditions.[29] In addition, the buried oxide quality and its variations across the wafer produces DGFETs with nonuniform electrical characteristics which hinder further scalability and optimization.[30−32] These limitations can be defeated with a new structure of dual-gate ISFETs with individually addressable or "true" back-gates fabricated by Taiwan Semiconductor Manufacturing Company (TSMC) with a 0.18 μm SOI technology. The new transistor is made in a two-stage process. First, the transistor is formed as a standard SOI metal-oxide-semiconductor FET (MOSFET). Then, the SOI wafer is flipped upside down and is attached to a new substrate. After removing the bulk silicon from the original SOI wafer, an opening is formed through the buried oxide to expose the back of the device silicon, and a high-k film is deposited to form the ISFET's gate dielectric. The resulting device then has two true gates—the front gate biased with a reference electrode in solution and the back-gate which is the poly gate of a standard foundry fabricated MOSFET. A schematic illustrating a cross section of the new device is presented in Figure 1. The full fabrication is performed in a standard semiconductor foundry leveraging high-quality materials and automated processes of CMOS manufacturing that enable traceable reliability with very high yields at a low cost. Furthermore, the devices have been integrated with control and read-out circuitry, making the full process amenable for immediate commercialization.

Besides enabling true back-gates, the new architecture improves electrical robustness and enables higher transistor density. Electrical interconnects (metals 1 and onward in a foundry process) are well isolated from the fluid with the original SOI buried oxide preventing leakage current from the metal leads to the fluid, which can be a crippling problem for

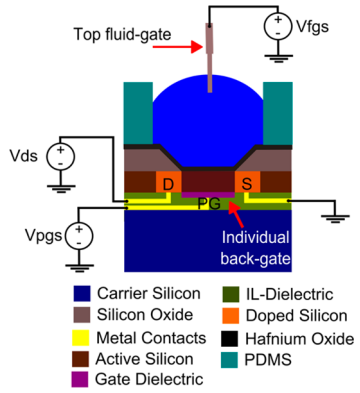

Figure 1. Schematic of the fabricated dual-gated ISFET. Cross-sectional view of the device and definition of biasing nomenclature. The color codes indicate materials of each layer in the terminated device.

thin deposited dielectric layers.[24] In addition, the new structure does not have a floating sensing gate preventing accumulation of charges and reducing the probability of sudden threshold voltage changes due to electrostatic discharge.[33,34] This novel device architecture also simplifies routing and increases possible transistor density because interconnect leads are in a different layer from the sensing regions. Figure S1 compares the cell footprint of single-gate transistors with the new structure. Because node connections are in a different layer and the extended gate is not used in the new structure, the developed true dual-gate transistors only occupy ∼25% of the area of the single-gate device which will impact transistor count. For sensing purposes, the new devices enable a tailored dual-gated operation that allows improvement of the signal-to-noise ratio (SNR). For defined pH ranges, increments in sensitivity overcome average noise resulting in enhanced pH resolution of the system. This characteristic is used to improve the sensor accuracy and decrease detection times when monitoring biological reactions. Using a loop-mediated isothermal DNA amplification,[35] we demonstrate that these devices enhance signals of biological reactions when operated in dual-gate mode enabling more accurate control and assessment. Due to the increased resolution of the configuration, the dual-gate mode yields a larger output signal in shorter detection times.

MATERIALS AND METHODS

Device Fabrication. The proposed dual-gate ISFET is manufactured on SOI wafers and was fabricated in entirety at TSMC with no additional post processing steps. Using standard complementary metal-oxide-semiconductor (CMOS) processing, the transistors are formed in the device layer. At this initial instance, devices are composed of a gate dielectric made of thermal silicon dioxide, a poly silicon gate, and source drain regions formed in a well with opposite doping. The formation of transistors is followed by deposition and patterning of multilayer interconnects (MLI) on the device substrate that create electrical connections to the source, drain, and gate nodes. The MLI structures comprise aluminum/copper conductive lines, tungsten vias, and are isolated with silicon dioxide interposing dielectric layers (ILD).

Following the MLI definition, a silicon handling wafer is bonded to the front side (exposed MLI and ILD layers) of the device substrate, and the wafer is flipped upside down. The bulk silicon layer of the original SOI wafer is then removed using a

dx.doi.org/10.1021/ac501912x | Anal. Chem. 2014, 86, 8359−8367

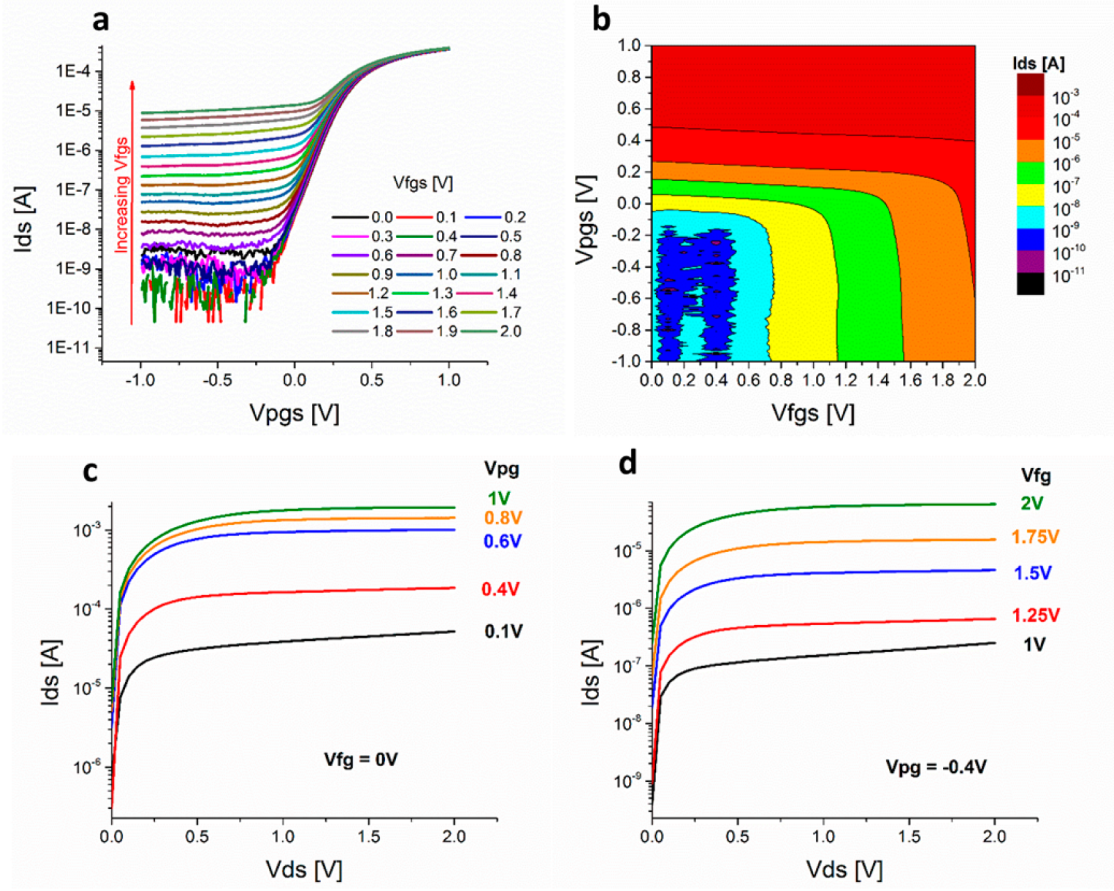

Figure 2. Electrical characterization of the transistor for fluid- and poly gate operations. (a) Current transfer characteristic (Ids vs Vpgs) for the poly gate under different fluid-gate biasing. The 2D heat map (b) shows the same information plotting drain current (logarithmic color code) as a function of fluid and poly gate biasing with Vds = 100 mV. FET transfer characteristic (Id vs Vds) of (c) the isolated bottom and (d) the top transistors under different gate biases.

chemical mechanical polish (CMP) process that uses the buried silicon oxide as an etch-stop layer. The now exposed buried oxide is etched in specific regions using standard photolithography and a wet etch to create windows that expose the back of the active silicon layer between the drain and source regions. It is then necessary to form the top-gate dielectric that will act as the sensing interface between the transistor and electrolyte. A seed layer of silicon dioxide followed by a thicker layer of hafnium oxide serve as the fluid-gate dielectric and sensing interface. The microfabrication process culminates with a photolithography and etch step that reveals the connection pads for device probing. Cross−sectional schematics of a summarized fabrication process are presented in the Supporting Information (Figure S2).

Measurement Setup. The electrical characterization of the fabricated dual-gated ISFETs was performed in a Keithley 4200 SCS with a filter factor of 1, delay factor of 1.3, and an automatic settling of the A/D aperture. These are the parameters of the "Quiet" acquisition mode, and different settings will change the measurement's noise. The device was probed in the configuration described in schematic in Figure 1, having independent SMUs for fluid (top) gate, poly(back) gate, and drain nodes, with all potentials referenced to a grounded source. A polydimethylsiloxane (PDMS) well is bonded to the front side of the transistor to act as a reservoir of the electrolyte that is biased with a leak-free reference electrode (Warner Instruments, Hamden, CT) connected to one of the SMUs to sweep or fix the fluid potential. The well is filled with a 10 mM PBS solution at different pH values or LAMP solution, Vds is set at 100 mV, and the two gates have different biases depending the desired operation mode.

pH Sensitivity Measurements. The pH sensitivity is evaluated for both the dual- and single-gate modes measuring changes of the surface potential as a function of pH. Solutions of 10 mM PBS are titrated with HCl and NaOH and measured with an Orion 3 star pH meter (Thermo Scientific, Pittsburgh, PA) to have five electrolytes of known pH. As will be discussed later in the Results and Discussion section, the dual-gate amplification mode limits the range of pH that can be measured. Therefore, the five testing electrolytes have pH values in the 6−9 range.

The prepared PBS solutions are manually pipetted in the PDMS well. After 5 min of stabilization, transfer characteristics are obtained in both the single- and dual-gate modes. For single-gate measurements, the bottom transistor is turned off by applying a negative potential to the poly gate, and the electrolyte potential is swept from 0 to 2 V. For the dual-gate mode, the top transistor is turned on applying an inversion bias while the poly gate is swept from −1 to 1 V. The drain current versus gate voltage transfer characteristic is obtained five times. The solution is then changed to the following pH value, and the procedure is repeated.

Pseudo Real-Time DNA Amplification Reaction. To test the benefits of the improved sensitivity and resolution, the

dx.doi.org/10.1021/ac501912x | *Anal. Chem.* 2014, 86, 8359−8367

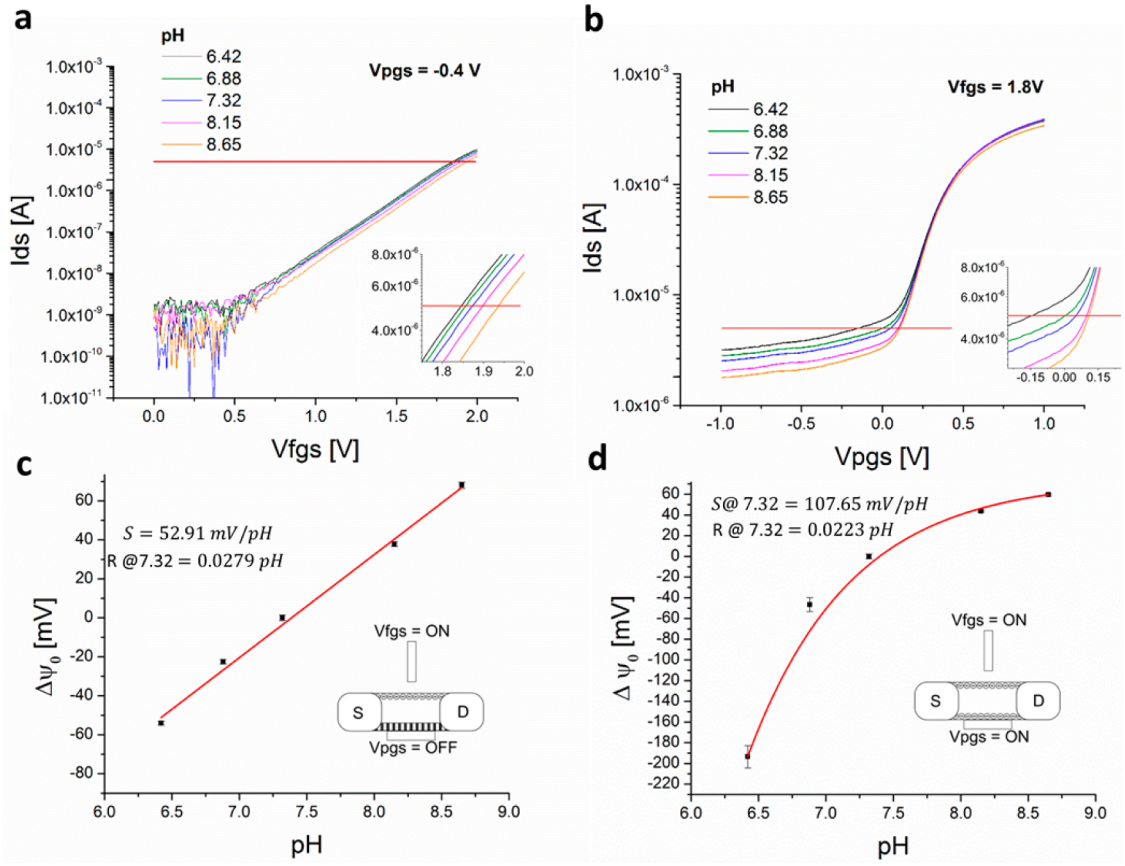

Figure 3. Measurement of transistor response to pH changes. (a) Transfer characteristics for the single-gate operation (Id vs Vfgs) and (b) transfer characteristic for the dual-gate operation (Id vs Vpgs) for five different pH values. The inset figures magnify to the voltage range where the threshold current is achieved. (c) Change in surface potential ($\Delta\psi_0$) as a function of electrolyte pH for the single-gate mode. (d) Change in surface potential ($\Delta\psi_0$) vs solution pH for the dual-gate operation. Each point is the average of five measurements, and the error bars are one standard deviation. Inset figures are schematics showing that in the single-gate mode only the top silicon is inverted and conducting while the bottom silicon is depleted, and in the dual-gate mode both top and bottom silicon are conducting.

dual-gate ISFETs were used to monitor a LAMP reaction. For each measurement, 100 μL of LAMP solution was prepared with the following components: 800 mM of Betaine (Sigma-Aldrich. St. Louis, MO), 1.4 mM of dNTP Mix (New England BioLabs, Ipswich, MA), 5 mM of Magnesium sulfate (Sigma-Aldrich), 50 mM Potassium chloride, 0.64 unit/mL of *Bacillus stearothermophilus* (Bst) 2.0 WarmStart polymerase (New England BioLabs), and 20 μM EvaGreen (Biotium, Hayward, CA). Additionally, the LAMP solution contains the primers for the *wzy* gene of Shiga toxing-producing *E. coli (STEC) O111* specified in Table S1 with the following concentrations 1.9 μM FIP/BIP, 0.24 μM F3/B3, and 0.96 μM Loop-B primers.[36,37] The positive samples had DNA extracted from an *STEC O111* overnight culture (Plating count of 9.1 × 10^8 CFU/ml), whereas the negative controls had additional DI water.

For a pseudo real-time study, identical LAMP solutions are heated to 63 °C for different time intervals in a Thermomixer R (Eppendorf, Hamburg). The solutions are cooled down in an ice bath for 1 min to stop the amplification reaction before measurements to quantify amplification are performed. Changes of the solution pH are measured with an Orion 3 star meter, and fluorescence changes related to increased binding sites for the intercalating dye are observed on a Nikon Eclipse FN-1 fluorescence microscope (Nikon Instruments, Inc., Melville, NY). The transistor threshold voltage is obtained from transfer characteristics taken for the dual- and single-gate modes. All three measurements are performed for each time interval for both negative and positive samples.

Data Analysis. The reported sensitivity is the derivative of the surface potential to pH function. For the single-gate mode, as it is usually done with ISFETs, the sensitivity is the slope "*b*" of the linear approximation $[f(x) = a + bx]$ to the pH response, where $f(x)$ is the surface potential and "*x*" the pH value. Therefore, the sensitivity remains constant for the different pH points. However, for the dual-gate operation, the surface potential to pH function is approximated with an exponential fit and an asymptotic model $[f(x) = a - b*c^2]$. The derivative of the model $[f'(x) = -b\, c^2 \ln(c)]$ is the sensitivity function that is evaluated for different pH points.

The pH resolution is defined as the ratio of noise over sensitivity.[28] Then, resolution in pH units is calculated as $\Delta\mathrm{pH}_{\min} = \sigma\psi_s/S$, where $\sigma\psi_s$ is the standard deviation of the measured surface potential and "*S*" is the sensitivity quantified as it was described above.

Finally, to compare the performance of dual- and single-gate operation modes for monitoring DNA amplification, a two-tail paired *P*-value was calculated comparing surface potential changes in positive samples with the respective negative controls. The number of compared points is accumulated with reaction time, comparing only initial measurements for *P*-value at 5 min and comparing the total number of points for the 60 min *P*-value. The *P*-value threshold is set at 0.01, which

dx.doi.org/10.1021/ac501912x | *Anal. Chem.* 2014, 86, 8359−8367

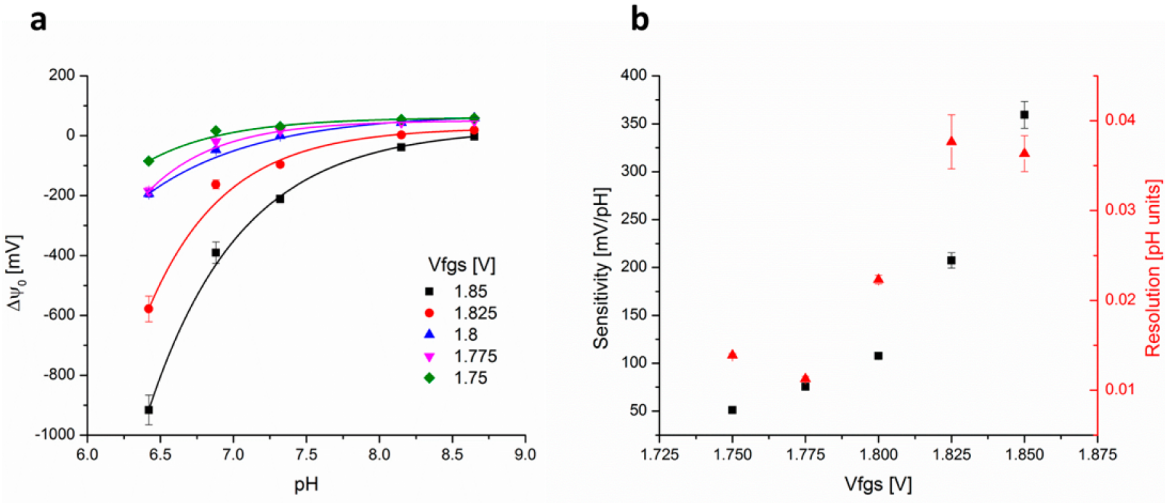

Figure 4. Tailoring fluid-gate bias to enhance resolution in the dual-gate mode. (a) Change in surface potential ($\Delta\psi_0$) as a function of electrolyte pH for multiple fluid-gate conditions. Each point is the average of five measurements, and the error bars are one standard deviation. (b) Sensitivity (squares) and resolution (triangles) for pH 7.32 in the dual-gate operation as a function of the electrolyte potential. Increments in fluid-gate potential increase the current ratio $\Delta I_{top}/\Delta I_{bottom}$, thereby increasing sensitivity. However, the noise is also larger limiting resolution improvements with larger sensitivities. For Vfgs = 1.775 V, we found an ideal biasing condition where the dual-gate SNR is about 2× larger than the one in single-gate operation. This improves the calculated sensor resolution for that pH operation from ∼0.03 to a finer 0.015 pH resolvable changes.

translates into a "very strong presumption" against a null hypothesis of having two identical samples.

RESULTS AND DISCUSSION

Device Electrical Characteristics. Figure 1 and 2 illustrate the device structure and basic electrical characterization. The schematic in Figure 1 describes the layers that compose the transistors including the attached PDMS well and the leak-free reference electrode. The nomenclatures for potentials are Vds for drain-source, Vpgs for the poly gate, and Vfgs for the fluid-gate. Figure 2a shows the Ids−Vpgs transfer characteristics of the double-gate operation sweeping the poly gate from −1 to 1 V and having several Vfgs. The same information is plotted in the contour heat map (Figure 2b) that summarizes the dependence of the drain current as a function of the fluid and poly gate biases. In Figure 2c,d, Vds is swept from 0 to 2 V for different gate biases showing typical resistive FET characteristics for the isolated top and bottom transistors. To isolate the transistors, the opposite gate is biased so it does not contribute to the drain current. This means that for poly gate transistor testing (Figure 2c), the fluid-gate is set to Vfgs = 0 V, and for fluid-gate testing (Figure 2d), the poly gate is set to a slight negative potential of Vpgs = −0.4 V. Figure 2b shows that at 0 V the conductivity of the bottom transistor is at tens of nanoamps, implying that at 0 V there are already inversion carriers in the poly gate side. Therefore, a negative potential is applied to the poly gate for completely shutting off the bottom current isolating the fluid-gate transistor.

Overall, the poly gate has better electrical characteristics than the fluid-gate side of the DGFET. The on/off ratio and saturation current are higher, whereas subthreshold swing and threshold voltage are lower for the poly gate side. Electrical characterization of top- and back-gates of multiple devices is presented in Figure S3. Measurements and extracted distributions show that a low noise and threshold variations are low for the back-gate, but their variability is larger top fluid-gate. This is expected because the gate dielectric on the poly gate side experiences highly optimized annealing steps to reduce oxide charge, compared to the fluid-gate's high-k dielectric, which is difficult to properly anneal at the end of processing. Furthermore, the fluid-gate is biased through the electrolyte where the capacitive coupling has a greater variability than in the poly gate.[38] Despite having the mentioned short-comings, the fluid-gate transistors have a near Nernstian sensitivity and high repeatability (mean threshold variation was only 10 mV in a stress test of 50 consecutive Id−Vg sweeps) for pH sensing.

Response to pH Changes. Sensitivity to pH changes was measured for dual- and single-gate modes as surface potential changes. For the fluid-gate mode, the electrolyte potential is swept, and the poly gate has a slight negative potential. On the other hand, in dual-gate operation, the fluid potential is set to create an inversion channel in the front side of the DGFET while the poly gate is swept. Figure 3a shows the single-gate Ids−Vfgs transfer characteristics for electrolytes with different pH values. The inset magnifies the region of voltages for a threshold current of 5 μA. Similarly, Figure 3b shows the Ids−Vpgs transfer characteristics for the dual-gate mode and an inset with magnification at threshold voltages. Figure 3c,d show the surface potential changes as a function of electrolyte pH with pH 7.32 as the origin or reference potential. Each point is an average of five measurements, and error bars are one standard deviation of the five measurements. The insets in Figure 3c,d are schematics illustrating that in the single-gate mode, only the front side transistor is inverted and conducting (Figure 3c), whereas in dual-gate mode, both sides are conducting (Figure 3d).

Figure 3c shows the typical linear response of the ISFET surface potential to pH changes, demonstrating a sensitivity of 52.91 mV/pH. On the other hand, Figure 3d shows a nonlinear response to pH for the dual-gate operation. The nonlinear behavior is explained by the fact that, as others have shown experimentally and theoretically,[23,39] the sensitivity to pH changes is a function of the drain current ratio of the coupled transistors $[\Delta I_{top}/\Delta I_{bottom}]$. Because for a fixed electrolyte potential the current ratio is a function of pH, the sensitivity is

dx.doi.org/10.1021/ac501912x | Anal. Chem. 2014, 86, 8359−8367

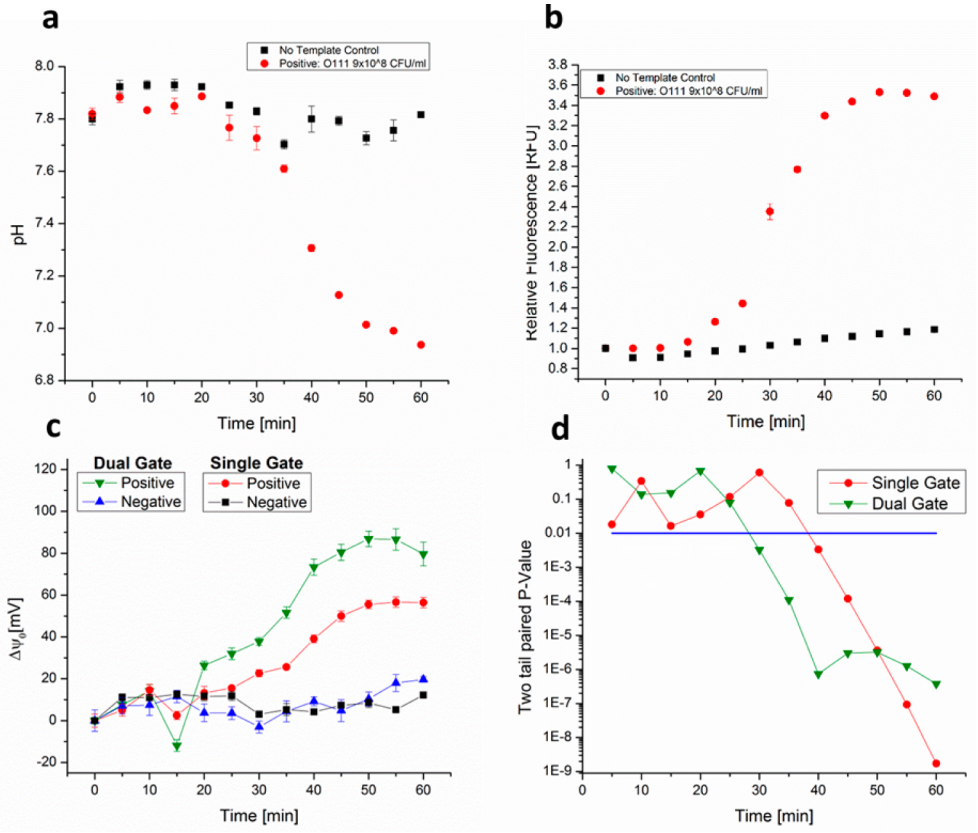

Figure 5. Pseudo real-time monitoring of LAMP DNA amplification of the *wzy* gene of *O111 STEC*. (a) Measured pH as a function of reaction time. (b) Fluorescence intensity as a function of reaction time. (c) Change in surface potential as a function of reaction time for the single- and dual-gate operation modes. All (a–c) show measurements for a positive sample with template DNA where amplification is expected and a negative control without template DNA where no amplification is expected. (d) Two-tail paired *P*-value as a function of reaction time for dual- and single-gate modes comparing their respective positive and negative samples. The dual-gate operation reduces the detection time by ∼10 min.

also a function of the solution's acidity. For instance, at a fixed potential, higher pH values will reduce the drain current in an N-type ISFET. Higher pH values are correlated with higher OH^- concentrations, which will reduce the number of inversion carriers in an N-type ISFET modifying the ratio of bottom/top transistor currents and consequently change pH sensitivity.

In addition, the surface potential to pH relation in the dual-gate mode shows an asymptotic behavior (Figure 3d). As the pH increases, the top transistor current decreases, and the poly gate side is forced to contribute more current to achieve the threshold that is used to extract the surface potential. The poly gate side of the device is not sensitive to the electrolyte pH, so the device loses sensitivity as the bottom transistor becomes the dominant source of drain current. Because at large pH values the top current is minimal, most of the drain current is coming from the bottom transistor, and therefore, the sensitivity approaches zero, explaining the asymptotic trend.

Figure 3d also shows that the dual-gate mode has sensitivities above the Nernstian limit for certain range of pH values. For example, the sensitivity (or derivative of the asymptotic model) at pH 7.32 is 107.65 mV/pH, and it increases for more acidic electrolytes. However, a greater sensitivity is also accompanied by larger noise. This is observed in Figure 3d by the larger error bars for lower pH values. Therefore, the ideal SNR or resolution is constrained to a window of pH values that is limited in one side by low sensitivities and in the other by large noise.

Tailoring of Biasing Conditions. The amplification of sensitivity does not necessarily improve resolution because larger sensitivities are accompanied by increased noise. Therefore, to enhance the signal-to-noise ratio, it is necessary to optimize the biasing condition to find operation points where the noise sources are not being amplified as much as the sensitivity.[28] Figure 4 presents the results of a resolution optimization experiment. Figure 4a illustrates the dual-gate mode surface potential to pH relationship for the same device under small differences of fluid-gate bias. Variations on the fluid bias modify the magnitude of drain current in the front transistor changing the current ratio and the pH sensitivity. Figure 4b quantifies the sensitivity and resolution at pH 7.32 for the different fluid biases (Table S2 presents the constants of the extracted models). As it is expected, the sensitivity increases with increments in Vfgs, because the top transistor contributes more to the threshold current. However, it is interesting to note that the optimal resolution is observed for Vfgs = 1.775 V. With this biasing, we obtain the best resolution of the five screened fluid biases. Figure S4 plots sensitivity, noise, and resolution as a function of the electrolyte pH, comparing the single-gate and the tailored dual-gate modes. With Vfgs = 1.775 V and for a specific pH range, gains in sensitivity are greater than noise increments. The sensitivity and resolution of the single-gate mode is also plotted in Figure S2 to compare the performance of both operations for electrolytes with different pH. When compared to the single-gate mode, the dual-gate mode exhibits an improvement in SNR of a factor of ∼2× for the 7.32 pH

dx.doi.org/10.1021/ac501912x | *Anal. Chem.* 2014, 86, 8359–8367

(from ~0.03 to 0.015 resolvable pH units). Similar exercises could be performed for other pH values to improve resolution for other electrolytes. Depending on experimental conditions like starting pH and expected pH change, the fluid-gate bias can be tailored to have optimal sensitivity and resolution.

To test the robustness and repeatability of the amplification method, the same pH characterization was done for five different transistors in both single- and dual-gate operation (Figure S5). In all devices, there is a pH range of improved resolution when operated in the tailored dual-gate mode. However, the magnitude and range of the sensitivity enhancement varies between transistors. Our measurements indicate that the resolution improves by 20.3% on average when compared with the single-gate operation; however, the standard is 19.1%. Variance in the top-gate threshold voltage and noise (as it is shown in Figure S3) may explain the lack of uniformity of the dual-gate resolution enhancement. However, the best resolution achieved with the tailored dual-gate operation is superior to the one required for DNA sequencing[20] and comparable to the inherently more sensitive nanowires.[40] Comparison of our results with other dual-gate approaches is complicated because as Rajan et al. mentioned, noise analysis has only been recently adopted by the FET-biosensor, and the reported sensitivity increments are not necessarily resolution improvements.

Monitoring of DNA Amplification Reactions. Improved sensitivity and resolution enables more precise monitoring of biological reactions. To illustrate this principle, we compared the response of dual- and single-gate modes when monitoring pH changes of DNA amplification reactions. The incorporation of dNTPs into a growing DNA strand causes the release of hydrogen ions and pyrophosphates.[20,41] This process has been thoroughly studied as a label-free sensing method of amplification and has been used for DNA sequencing[42] and detection of specific mutations.[43]

Experiments in Figure 5 show pseudo real-time amplification of the *wzy* gene of O111 *STEC* using LAMP.[36] Starting in 2011, the U.S. Department of Agriculture initiated a zero tolerance policy for a group of 6 non O157 *STECs*.[44] The O111 serotype is part of this so-called "big six group" and has caused multiple outbreaks thereby becoming an important target for food safety control.[45,46] Our lab has investigated detection methods for the "big six" strands and the O111 type was used to evaluate and compare the performance of the single- and dual-gate operation of the fabricated ISFETs for monitoring a LAMP reaction.

DNA amplification and simultaneous measurement of the transistor surface potential presented challenges that hinder the comparison of dual- and single-gate modes. First, the heated stage that is used for on-chip amplification (mK1000 heated stage from Instec, Bouler, CO) introduces new sources of noise that overshadow the small pH signals coming from the amplification reaction. Second, when performed on the silicon materials the DNA amplification reactions have lower yields due to nonspecific adsorption of molecules that reduce the measured signal.[47,48] Third, even though the solution is capped with mineral oil, the evaporation through the PDMS well causes a concentration of products that increases experimental noise. Therefore, a pseudo real-time LAMP (described in the methods sections) is performed to have a controlled experiment to evaluate the benefits of dual-gate ISFETs for reaction monitoring.

Figure 5a shows the measured LAMP solution pH as a function of time, Figure 5b shows relative fluorescence for positive and negative samples (Figure S6 shows the fluorescence images), and Figure 5c shows the surface potential change for dual- and single-gate modes as a function of time. Figure 5a,b shows that solutions where amplification is expected turn more acidic and increase fluorescence intensity with reaction time. On the other hand, Figure 5c shows that the surface potential is maintained relatively constant for negative solutions, whereas measurements of positive solutions induce surface potential changes as a function of time. This means that the surface potential responds to pH changes induced by nucleotide incorporation which occurs only in LAMP samples with template DNA. The larger sensitivity of the dual-gate mode, which is achieved by tailoring the top and bottom current ratio of the device at the beginning of the experiment, produces surface potential changes that are larger than the ones in single-gate operation. This translates into a faster detection time because the dual-gate mode enables the differentiation of negative and positive samples faster than the single-gate operation. Figure 5d shows the two tailored *P*-value calculated to compare negative and positive solutions for the dual and single-gate modes. The threshold is set at 0.01 or in other words when the null hypothesis of having two equal samples is rejected with 99% confidence. The *P*-value shows that the dual-gate operation allows us to establish statistical conclusions about 10 min faster than with the single-gate operation.

This result demonstrates the benefits of having an amplified sensitivity especially in high-noise environments or protocols. For the pseudo real-time measurements, the dominant source of noise is not coming from the device itself but the measurement protocol and setup. Each time point is a different solution that was measured individually. This means that for each measurement, there are small experimental changes like probe contact resistance, position of the reference electrode, and temperature changes that will introduce experimental noise to the surface potential measurement. In fact, these experimental variations become the dominant source of noise. The noise in experiments for pH characteristics (Figure 3) was in the order of 4 mV, and the one for the DNA amplification experiment is about 12−19 mV. The experimental noise is not being amplified by the dual-gate operation, and therefore, a higher resolution is achieved with amplified sensitivity. Go et al. had similar predictions and observations when modeling dual-gate operation.[23,28] If the sensor signal-to-noise ratio is limited by extrinsic sources of noise, the dual-gate offers superior resolution, because the sensitivity increases without significant noise amplification. Go et al. discussed the role of instrumentation noise, and here we observe a similar extrinsic noise source, which is the experimental procedure. In this case, the increased sensitivity amplifies the signal from the pH amplification without significant noise increments, and in consequence, differentiation of negative and positive samples is faster for the dual-gate operation. This demonstrates that the signal amplification of the dual-gate operation allows improved monitoring of reactions, especially in noisy environments, enabling observation of smaller pH signals or reducing the reaction time needed to make conclusions. These attributes of the dual-gate mode are especially desirable for point-of-care and on-site applications. Diagnostic assessments that are performed outside a controlled environment (i.e., not in a standard laboratory) are required to operate under more aggressive extrinsic sources of noise and with low-precision instrumentation.[49] Then, for these applications, the dominant source of noise will not be amplified in the dual-gate operation, enabling

dx.doi.org/10.1021/ac501912x | *Anal. Chem.* 2014, 86, 8359−8367

greater resolution improvements. In addition, the improved detection time of the dual-gate operation enables a faster turnaround diagnosis that is essential for portable applications where subsequent actions are contingent on diagnosis.[50] Therefore, it is in the portable applications where true dual-gated ISFETs can provide greater SNR amplification improving the device performance. However, data in Figure 5c,d also demonstrate that the increased sensitivity is accompanied by a loss of linearity and a consequent reduction in dynamic range. After 40 min, the dual-gate response changes the trend of improved SNR, suggesting that the new pH of the LAMP solution is outside the operation range, where the dual-gate mode has improved resolution. Therefore, gains in sensitivity and resolution are offset by reductions in dynamic range and linearity of response.

CONCLUSIONS

We have presented a dual-gated ISFET with a true back-gate where the coupling of front and back transistors enables pH sensitivity amplification and enhanced resolution for determined biasing conditions and ranges. A novel fabrication protocol produces a standard MOSFET as the back-gate transistor, and a high-K dielectric is used to interface the front-gate transistor with the electrolyte. The devices are made in a conventional semiconductor foundry, the fabrication process and the device structure is suitable for rapid scalability and seamless incorporation of other electronic components. These transistors were operated in single- and dual-gate modes for pH measurements and biological reaction monitoring. The single-gate mode operation has the same linear pH response characteristics of regular ISFETs, but when operated in dual-gate mode, the sensor response to pH becomes asymptotic due to the dynamic current ratios for different pH values. We show that for certain pH range, the dual-gate sensitivity is amplified more than the noise, yielding a higher SNR and enhanced resolution. Furthermore, we demonstrate that the operation point can be tailored by manipulating the fluid bias to maximize the SNR for a specific pH range and application.

We used the fabricated ISFETs to monitor a LAMP DNA amplification reaction in single- and dual-gate modes. The pH changes related to incorporation of nucleotides change the surface potential of the transistor enabling electrical label-free detection of DNA replication that is better monitored with the dual-gate operation. For the presented experiment, the noise is dominated by an extrinsic source and the greater sensitivity of the dual-gate mode yields an improved resolution that reduces the detection time which is established when the negative and positive samples are clearly differentiated. This new device and the dual-gate operation can be used as an electrochemical transducer for biological sensors that enable signal enhancement for better monitoring of reactions. The new structure has particular potential for applications targeting point-of-care diagnosis that are subject to noisy environments and require a fast turnaround. Future work will aim to maximize the resolution improvement and the pH range of operation of the dual-gated ISFETS by optimizing W/L ratio, top/bottom capacitances, and using arrays of devices to monitor the reactions.

ASSOCIATED CONTENT

Supporting Information

Additional information as noted in text. This material is available free of charge via the Internet at http://pubs.acs.org/.

AUTHOR INFORMATION

Corresponding Authors

*E-mail: rbashir@illinois.edu. Tel.: 217-333-3097.
*E-mail: ysliuj@tsmc.com. Tel.: 886-3-5636688.

Author Contributions

▲C.D.-G. and F.-L.L. contributed equally.

Notes

The authors declare no competing financial interest.

ACKNOWLEDGMENTS

We would like to acknowledge support of TSMC's MEMS and DTP teams and Dr. Chia-Hsien Hsu and his laboratory staff at National Health Research Institute in Zhunan, Taiwan. In addition we acknowledge funding support from Taiwan Semiconductor Manufacturing Company (TSMC) under contract TSMC-2012-06536, and from a cooperative agreement with Purdue University and the Agricultural Research Service of the United States Department of Agriculture, project number 1935-42000-035, and a subcontract to the University of Illinois at Urbana−Champaign.

REFERENCES

(1) Bergveld, P. *IEEE Trans.* **1970**, *1*, 70−71.
(2) Toumazou, C.; Georgiou, P. *Electron. Lett.* **2011**, *47*, S7−S12.
(3) Bergveld, P. *Sens. Actuators, B* **2003**, *88*, 1−20.
(4) Balasubramanian, K. *Biosens. Bioelectron.* **2010**, *26*, 1195−1204.
(5) Cui, Y.; Wei, Q.; Park, H.; Lieber, C. M. *Science* **2001**, *293*, 1289−1292.
(6) Dorvel, B. R.; Reddy, B.; Go, J.; Duarte Guevara, C.; Salm, E.; Alam, M. A.; Bashir, R. *ACS Nano* **2012**, *6*, 6150−6164.
(7) Penner, R. M. *Annu. Rev. Anal. Chem.* **2012**, *5*, 461−485.
(8) Chen, Y.; Star, A.; Vidal, S. *Chem. Soc. Rev.* **2013**, *42*, 4532−4542.
(9) Lei, J.; Ju, H. *Wiley Interdiscip. Rev.: Nanomed. Nanobiotechnol.* **2010**, *2*, 496−509.
(10) Ahuja, T.; Kumar, D. *Sens. Actuators, B* **2009**, *136*, 275−286.
(11) Li, X.; Chin, E.; Sun, H.; Kurup, P.; Gu, Z. *Sens. Actuators, B* **2010**, *148*, 404−412.
(12) Pal, S.; Alocilja, E. C.; Downes, F. P. *Biosens. Bioelectron.* **2007**, *22*, 2329−2336.
(13) Lung Khung, Y.; Narducci, D. *Biosens. Bioelectron.* **2013**, *50*, 278−293.
(14) Makowski, M. S.; Ivanisevic, A. *Small* **2011**, *7*, 1863−1875.
(15) Kim, D.-J.; Lee, N.-E.; Park, J.-S.; Park, I.-J.; Kim, J.-G.; Cho, H. J. *Biosens. Bioelectron.* **2010**, *25*, 2477−2482.
(16) Stern, E.; Vacic, A.; Li, C.; Ishikawa, F. N.; Zhou, C.; Reed, M. a; Fahmy, T. M. *Small* **2010**, *6*, 232−238.
(17) Kim, J.-Y.; Choi, K.; Moon, D.-I.; Ahn, J.-H.; Park, T. J.; Lee, S. Y.; Choi, Y.-K. *Biosens. Bioelectron.* **2013**, *41*, 867−870.
(18) Gong, J.-R. *Small* **2010**, *6*, 967−973.
(19) Al-Ahdal, A.; Toumazou, C. *Sens. Actuators, B* **2012**, *171−172*, 110−117.
(20) Rothberg, J. M.; Hinz, W.; Rearick, T. M.; Schultz, J.; Mileski, W.; Davey, M.; Leamon, J. H.; Johnson, K.; Milgrew, M. J.; Edwards, M.; Hoon, J.; Simons, J. F.; Marran, D.; Myers, J. W.; Davidson, J. F.; Branting, A.; Nobile, J. R.; Puc, B. P.; Light, D.; Clark, T. a; Huber, M.; Branciforte, J. T.; Stoner, I. B.; Cawley, S. E.; Lyons, M.; Fu, Y.; Homer, N.; Sedova, M.; Miao, X.; Reed, B.; Sabina, J.; Feierstein, E.; Schorn, M.; Alanjary, M.; Dimalanta, E.; Dressman, D.; Kasinskas, R.; Sokolsky, T.; Fidanza, J. a; Namsaraev, E.; McKernan, K. J.; Williams, A.; Roth, G. T.; Bustillo, J. *Nature* **2011**, *475*, 348−352.
(21) Kalofonou, M.; Toumazou, C. *Sens. Actuators, B* **2013**, *178*, 572−580.
(22) Wang, J. *Biosens. Bioelectron.* **2006**, *21*, 1887−1892.
(23) Go, J.; Nair, P. R.; Reddy, B., Jr.; Dorvel, B. *ACS Nano* **2012**, *6*, 5972−5979.

(24) Knopfmacher, O.; Tarasov, A.; Fu, W.; Wipf, M.; Niesen, B.; Calame, M.; Schönenberger, C. *Nano Lett.* **2010**, *10*, 2268−2274.
(25) Spijkman, M.-J.; Brondijk, J. J.; Geuns, T. C. T.; Smits, E. C. P.; Cramer, T.; Zerbetto, F.; Stoliar, P.; Biscarini, F.; Blom, P. W. M.; de Leeuw, D. M. *Adv. Funct. Mater.* **2010**, *20*, 898−905.
(26) Khamaisi, B.; Vaknin, O.; Shaya, O.; Ashkenasy, N. *ACS Nano* **2010**, *4*, 4601−4608.
(27) Lim, H.-K.; Fossum, J. G. *IEEE Trans.* **1983**, *30*, 1244−1251.
(28) Go, J.; Nair, P. R.; Alam, M. A. *J. Appl. Phys.* **2012**, *112*, 34516.
(29) Tarasov, A.; Fu, W.; Knopfmacher, O.; Brunner, J.; Calame, M.; Schönenberger, C. *Appl. Phys. Lett.* **2011**, *98*, 012114.
(30) Gao, Z.; Agarwal, A.; Trigg, A. D.; Singh, N.; Fang, C.; Tung, C.-H.; Fan, Y.; Buddharaju, K. D.; Kong, J. *Anal. Chem.* **2007**, *79*, 3291−3297.
(31) Rajan, N. K.; Duan, X.; Reed, M. A. *Wiley Interdiscip. Rev.: Nanomed. Nanobiotechnol.* **2013**, *5*, 629−645.
(32) Gu, Y.; Vu, T.; Li, G. P. In *SOI Conf., Proc. of the IEEE Int.*, Tucson, AZ, October 3−5, 1995; pp 94−95.
(33) Baldi, A.; Bratov, A.; Mas, R.; Dominguez, C. *Sens. Actuators, B* **2001**, *80*, 255−260.
(34) Liu, Y.; Georgiou, P.; Constandinou, T. G.; Garner, D.; Toumazou, C. In *Proc. IEEE Int. Symp. Circuits Syst.*, Taipei, Taiwan, May 24−27, 2009; pp 1165−1168.
(35) Notomi, T.; Okayama, H.; Masubuchi, H.; Yonekawa, T.; Watanabe, K.; Amino, N.; Hase, T. *Nucleic Acids Res.* **2000**, *28*, E63.
(36) Duarte, C.; Salm, E.; Dorvel, B.; Reddy, B.; Bashir, R. *Biomed. Microdevices* **2013**, *15*, 821−830.
(37) Wang, F.; Jiang, L.; Yang, Q.; Prinyawiwatkul, W.; Ge, B. *Appl. Environ. Microbiol.* **2012**, *78*, 2727−2736.
(38) Liu, Y.; Georgiou, P.; Prodromakis, T.; Constandinou, T. G.; Toumazou, C. *IEEE Trans.* **2011**, *58*, 4414−4422.
(39) Spijkman, M.; Smits, E. C. P.; Cillessen, J. F. M.; Biscarini, F.; Blom, P. W. M.; de Leeuw, D. M. *Appl. Phys. Lett.* **2011**, *98*, 043502.
(40) Rajan, N. K.; Brower, K.; Duan, X.; Reed, M. A. *Appl. Phys. Lett.* **2014**, *104* (8), 084106.
(41) Credo, G. M.; Su, X.; Wu, K.; Elibol, O. H.; Liu, D. J.; Reddy, B.; Tsai, T.-W.; Dorvel, B. R.; Daniels, J. S.; Bashir, R.; Varma, M. *Analyst.* **2012**, *137*, 1351−1362.
(42) Merriman, B.; Ion Torrent R&D Team; Rothberg, J. M. *Electrophoresis* **2012**, *33*, 3397−3417.
(43) Toumazou, C.; Shepherd, L. M.; Reed, S. C.; Chen, G. I.; Patel, A.; Garner, D. M.; Wang, C.-J. A.; Ou, C.-P.; Amin-Desai, K.; Athanasiou, P.; Bai, H.; Brizido, I. M. Q.; Caldwell, B.; Coomber-Alford, D.; Georgiou, P.; Jordan, K. S.; Joyce, J. C.; La Mura, M.; Morley, D.; Sathyavruthan, S.; Temelso, S.; Thomas, R. E.; Zhang, L. *Nat. Methods* **2013**, *10*, 641−646.
(44) Luchansky, J. B.; Porto-Fett, A. C. S.; Shoyer, B. A.; Phillips, J.; Eblen, D.; Evans, P.; Bauer, N. *J. Food Prot.* **2013**, *76*, 1434−1437.
(45) Bradley, K. K.; Williams, J. M.; Burnsed, L. J.; Lytle, M. B.; McDermott, M. D.; Mody, R. K.; Bhattarai, A.; Mallonee, S.; Piercefield, E. W.; McDonald-Hamm, C. K.; Smithee, L. K. *Epidemiol. Infect.* **2012**, *140*, 1644−1654.
(46) Piercefield, E. W.; Bradley, K. K.; Coffman, R. L.; Mallonee, S. M. *Arch. Int. Med.* **2010**, *170*, 1656−1663.
(47) Erill, I.; Campoy, S.; Erill, N.; Barbé, J.; Aguiló, J. *Sens. Actuators, B* **2003**, *96*, 685−692.
(48) Asiello, P. J.; Baeumner, A. J. *Lab Chip* **2011**, *11*, 1420−1430.
(49) Myers, F. B.; Lee, L. P. *Lab Chip* **2008**, *8*, 2015−2031.
(50) Hsieh, Y.-H.; Hogan, M. T.; Barnes, M.; Jett-Goheen, M.; Huppert, J.; Rompalo, A. M.; Gaydos, C. A. *PLoS One* **2010**, *5*, e14144.